BODIPY Nanoparticles Functionalized With Lactose for Cancer-Targeted and Fluorescence Imaging-guided Photodynamic Therapy

Duy Khuong Mai
Chonnam National University
Chanwoo Kim
Yonsei University
Joomin Lee
Chosun University
Temmy Pegarro Vales
Caraga State University
Isabel Wen Baldon
Chosun University
Cho Sung
Chonnam National University
Jaesung Yang
Yonsei University
Ho-Joong Kim (hjkim@chosun.ac.kr)
Chosun University

Research Article

Keywords: para-phenyl moiety, PeT process, photophysical properties, BODIPY, water-soluble nanoparticles (NPs)

Posted Date: August 26th, 2021

DOI: https://doi.org/10.21203/rs.3.rs-833734/v1

Version of Record: A version of this preprint was published at Scientific Reports on February 15th, 2022.
See the published version at https://doi.org/10.1038/s41598-022-06000-5.

Abstract

A series of four lactose-modified BODIPY photosensitizers (PSs) with different substituents (-I, -H, -OCH_3, and -NO_2) in the *para*-phenyl moiety attached to the *meso*-position of the BODIPY core were synthesized; the photophysical properties and photodynamic anticancer activities of these sensitizers were investigated, focusing on the electronic properties of the different substituent groups. Iodine substitution (BODIPY **I**) enhanced the intersystem crossing (ISC) to produce singlet oxygen ($^1O_2$) due to the heavy atom effect, and maintained a high fluorescence quantum yield (Φ_F) of 45.3%. Substitution with the electron-donating group (-OCH_3) (BODIPY **OMe)** resulted in a high $^1O_2$ generation capability and a Φ_F of 49.2% while substitution with the electron-withdrawing group (-NO_2) led to the PeT process. Thus, instead of assisting ISC as typically expected, this BODIPY PS induced non-radiative charge recombination, prohibiting both fluorescence emission and $^1O_2$ generation. The BODIPY PSs formed water-soluble nanoparticles (NPs) functionalized with lactose as liver cancer-targeting ligands. BODIPY **I** and **OMe** NPs showed good fluorescence imaging and PDT activity against various tumor cells (HeLa and Huh-7 cells). Collectively, the BODIPY NPs demonstrated high $^1O_2$ generation capability and Φ_F may create a new opportunity to develop useful imaging-guided PDT agents for tumor cells.

Introduction

Photodynamic therapy (PDT) is a promising cancer treatment that has been applied to various cancers, such as oral, lung, bladder, brain, ovarian, and esophageal cancers[1,2]. The PDT process requires three key components: light, oxygen, and a photosensitizing agent[3]. In the presence of absorbed light, the photosensitizer (PS) initiates a photochemical reaction with oxygen, resulting in cytotoxic reactive oxygen species (ROS), such as singlet oxygen ($^1O_2$), which directly kills tumor cells[4,5]. PDT can provide good selectivity and is non-invasive at the treatment region as the activity of this medical technique is only carried out when the PS is combined with light of a particular wavelength. Recently, imaging-guided PDT has been assessed to develop specific agents for visualizing individual tumor targets, thereby enhancing therapeutic efficiency and reducing side effects[6]. However, to date, PSs that can be simultaneously applied for both imaging and treatment are not available in the clinic. Accordingly, there is an urgent need to develop PSs that can effectively produce both fluorescence and ROS[7,8].

Among the different PSs, 4, 4-difluoro-4-bora-3a,4a-diaza-s-indacene (BODIPY) is a new family of fluorescent dyes with outstanding photophysical features, such as high molar extinction coefficient, high quantum efficiencies of fluorescence, and easy modification. BODIPYs have thus been applied as promising imaging/detection agents with high light-to-dark toxicity ratios[9–12]. The generation of $^1O_2$ in solution requires PS to be converted to the triplet excited state (intersystem crossing, ISC) upon irradiation. Many dyes with a high ISC obtained from natural or synthetic sources have been employed in PDT reactions[13,14]. The most common design strategy employed to enhance ISC is the conjugation of heavy halogen atoms (Br or I) to promote spin-orbit coupling (SOC), which improves the $^1O_2$ generation

capability and the population of longer-lived excited triplet states[15,16]. However, the incorporation of heavy halogen atoms causes toxicity and fluorescence quenching[11,17,18]. Therefore, BODIPY PSs without heavy halogen atoms are preferred as theranostic agents.

Several approaches with heavy-atom-free PSs to improve the ISC, such as the use of dimer BODIPY[19,20], spin converters[21], and photoinduced electron transfer (PeT)[22,23], have recently been reported. The formation of triplet states via photoinduced electron transfer (PeT) is a well-known process that was not employed to develop practical triplet sensitizers until recently[24]. The charge-transfer (CT) states comprised the donor radical cation and the acceptor radical anion are induced by PeT, which recombines the ground state *via* different pathways[23,25,26]. Owing to its high dipole moment, the energy of the CT states strongly depends on the polarity of the media. In non-polar solvents, the CT energy level is usually significantly higher than that of the dyad's first excited state, resulting in very low PeT efficiency and intense fluorescence. In contrast, for solvents with sufficient polarity, such as in an aquatic environment, the CT state energy is reduced, causing PeT and the triplet state[27], which ultimately induce fluorescence quenching and forbid singlet oxygen generation.

Recently, we reported a series of water-soluble BODIPY PSs attached to heavy atoms at the 2,6-position of the BODIPY core[17]. These BODIPY PSs showed excellent PDT ability, while exhibiting very low dark toxicity; however, they could not be used as imaging reagents due to their low fluorescence quantum yield (Φ_F) resulting from the incorporation of heavy atoms. To overcome the above-mentioned issues, we aim to develop heavy-atom-free BODIPY PSs with imaging-guided PDT properties. Herein, we present a new family of heavy-atom-free BODIPY nanoparticles (NPs) (Scheme 1) with potential applications in tumor-targeted fluorescence cell imaging and PDT. We synthesized four BODIPY PSs containing different substituent groups (-I, -H, -OCH_3, and -NO_2) in the *para*-phenyl moiety attached to the *meso*-position of the BODIPY core, and investigated their photophysical and photosensitizing properties according to the variation in the substituents. In addition, BODIPY segments were conjugated with lactose-tethering triazole as a specific ligand for asialoglycoprotein (ASGP) in liver cancer cells[28]. The resulting BODIPY PSs formed NPs with a uniform size in water. Further, the cell viability, cellular imaging, and photodynamic anticancer activities of these BODIPY NPs were evaluated using HeLa and Huh-7 cells. Overall, our findings indicate that BODIPY NPs are promising tumor-targeted PDT agents, with fluorescence cell imaging properties in live cancer cell lines.

Methods

Materials Instrumentations

Almost all reagents and chemicals were obtained from Sigma Aldrich (St. Louis, MO, USA). Some solvents such as dichloromethane (CH_2Cl_2), methanol (MeOH), or $MgSO_4$, sodium azide (NaN_3), sodium ascorbate (NaAsc), Copper (II) sulfate pentahydrate ($CuSO_4.5H_2O$) were purchased from Daejung

chemical (Gyeonggi-do, South Korea), and used without further purification. Lactose-propargyl was synthesized in our previous literature[17].

All compounds were characterized by ^{1}H and ^{13}C-NMR spectroscopy on a Bruker AM 250 spectrometer (Billerica, MA, USA). The impurity of the products was checked by thin-layer chromatography (TLC, silica gel 60 mesh). UV spectra were measured on a Shimadzu UV-1650PC spectrometer, and Fluorescence spectra were carried on a Hitachi F-7000 spectrometer. The size and morphology of BODIPY NPs were analyzed by using dynamic light scattering (DLS) on Malvern Zetasizer Nano ZS90 and transmission electron microscopy (TEM). We used machine JEOL- JEM 2100F at an accelerating voltage of 200 kV. The sample for TEM was prepared according to our reported literature[41].

Synthesize of water-soluble BODIPY I, H, OMe, and NO2:

According to our reported literature[17], the series of water-soluble BODIPY **I**, **H**, **OMe**, and **NO2** were prepared using the same pathway. A representative routine is presented for the compound **I**. Briefly, BODIPY **2a** (80 mg, 0.157 mmol), lactose propargyl (66 mg, 0.173 mmol), NaAsc (156 mg, 0.785 mol), and $CuSO_4.5H_2O$ (79 mg, 0.316 mmol) were dissolved in the mixture of THF/water (15/5 mL, v/v). The resulting mixture was stirred for one day at room temperature, extracted with THF and water three times, and dried over $MgSO_4$. After removing the solvent by a rotary evaporator, the crude product was purified by recrystallization using MeOH/diethyl ether to afford an orange solid (yield 76 mg, 52% yield). ^{1}H NMR (300MHz, CD_3OD, δ, ppm): δ 8.02 (s, 1H), 7.97- 7.95 (d, 2H), 7.17- 7.15 (d, 2H), 5.83 (s, 2H), 4.36- 4.33 (d, 2H), 3.87- 3.85 (d, 2H), 3.81- 3.80 (d, 2H), 3.76- 3.74 (d, 1H), 3.71- 3.69 (d, 1H), 3.57- 3.53 (d, 2H), 3.49- 3.48 (d, 2H), 3.31- 3.29 (d, 2H), 2.57 (s, 3H), 2.42-2.39 (q, 4H), 1.44 (s, 3H), 1.36 (s, 3H), 1.28 (s, 3H), 1.05- 1.00 (t, 3H). ^{13}C NMR (75MHz, CD_3OD, δ, ppm): δ 162.25, 143.55, 143.24, 142.81, 140.13, 138.60, 137.3, 135.75, 134.58, 134.16, 131.48, 131.32, 105.09, 103.29, 96.18, 80.57, 77.05, 76.45, 76.29, 74.75, 74.58, 72.52, 70.38, 63.00, 62.42, 61.82, 46.12, 17.57, 17.32, 14.87, 14.76, 13.2, 12.45, 11.92. HRMS (ESI): calculated for ($C_{38}H_{49}BF_2IN_5O_{11}$): m/z: [M]: 928.2613; found: 928.2619.

Compound H: BODIPY **H** was synthesized according to the general procedure to afford the orange solid (67 mg, 57% yield). ^{1}H NMR (300MHz, CD_3OD, δ, ppm): δ 8.01 (s, 1H), 7.59- 7.57 (t, 3H), 7.37- 7.36 (d, 2H), 5.84 (s, 2H), 4.37- 4.33 (d, 2H), 3.87- 3.85 (d, 2H), 3.81- 3.80 (d, 2H), 3.76- 3.73 (d, 1H), 3.69- 3.66 (d, 1H), 3.59- 3.57 (d, 2H), 3.54- 3.52 (d, 2H), 3.49- 3.32 (d, 2H), 2.53 (s, 3H), 2.43-2.38 (q, 4H), 1.38 (s, 3H), 1.31 (s, 3H), 1.28 (s, 3H), 1.04- 0.99 (t, 3H). ^{13}C NMR (75MHz, CD_3OD, δ, ppm): δ 161.82, 144.19, 143.61, 143.46, 138.71, 136.45, 134.29, 131.7, 130.75, 130.61, 129.43, 105.16, 103.36, 80.45, 77.26, 77.15, 76.41, 74.6, 72.4, 70.26, 62.96, 62.53, 61.77, 61.66, 48.07, 17.68, 14.85, 14.5, 13.16, 12.24, 11.66. HRMS (ESI): calculated for ($C_{38}H_{55}BF_2IN_5O_{12}Na$): m/z: $[M+Na]^+$: 834.3713; found: 834.3714.

Compound OMe: BODIPY **OMe** was synthesized according to the general procedure to afford the orange solid (55 mg, 47 % yield). ^{1}H NMR (300MHz, CD_3OD, δ, ppm): δ 8.0 (s, 1H), 7.23- 7.2 (d, 2H), 7.13- 7.1 (d, 2H), 5.87 (s, 2H), 4.37- 4.34 (d, 2H), 3.89 (s, 3H), 3.77- 3.71 (q, 3H), 3.6- 3.5 (m, 6H), 3 42- 3.39 (d, 1H), 2.56

(s, 3H), 2.4-2.38 (q, 4H), 1.43 (s, 3H), 1.36 (s, 3H), 1.28 (s, 3H), 1.01- 0.95 (t, 3H). ^{13}C NMR (75MHz, CD_3OD, δ, ppm): δ 162.15, 144.48, 143.03, 138.59, 136.87, 134.71, 134.18, 132.17, 130.55, 128.29, 116.06, 105.04, 103.33, 80.37, 77.08, 76.53, 76.22, 74.82, 74.64, 72.64, 70.21, 63.04, 62.43, 61.75, 55.8, 46.14, 17.73, 17.44, 14.87, 14.26, 13.28, 12.53, 11.56. HRMS (ESI): calculated for ($C_{39}H_{52}BF_2N_5O_{12}Na$): m/z: $[M+Na]^+$: 854.3571; found: 854.3572.

Compound NO2: BODIPY **NO2** was synthesized according to the general procedure to afford the orange solid (80 mg, 61 % yield). ^{1}H NMR (300MHz, CD_3OD, δ, ppm): δ 8.47- 8.44 (d, 2H), 8.01 (s, 1H), 7.69- 7.66 (d, 2H), 5.83 (s, 2H), 4.37- 4.34 (d, 2H), 3.86- 3.32 (d, 2H), 3.79- 3.75 (d, 2H), 3.6- 3.5 (m, 6H), 3.31- 3.29 (d, 2H), 2.59 (s, 3H), 2.41- 2.39 (q, 4H), 1.39 (s, 3H), 1.31 (s, 3H), 1.29 (s, 3H), 1.04- 0.98 (t, 3H). ^{13}C NMR (75MHz, CD_3OD, δ, ppm): δ 163.11, 149.96, 143.16, 141.37, 138.46, 137.78, 134.63, 133.69, 131.64, 130.96, 125.76, 105.14, 103.6, 80.37, 77.35, 76.4, 76.24, 74.84, 74.35, 72.54, 70.36, 63.11, 62.44, 61.76, 46.06, 19.39, 17.86, 14.86, 14.46, 13.09, 12.63, 11.71. HRMS (ESI): calculated for ($C_{38}H_{49}BF_2N_6O_{13}Na$): m/z: $[M+Na]^+$: 869.3316; found: 869.3318.

Measurement of photophysical properties

The Φ_f were measured by a comparative method using the standard reference with the already-known value of Φ_f as follows:

$$\Phi_S = \Phi_R \left(\frac{A_R}{A_S}\right)\left(\frac{n_S}{n_R}\right)^2\left(\frac{D_S}{D_R}\right)$$

The subscript of S and R represent sample and reference, respectively. N is the refractive index of solvent. A and D are the absorbance and the integrated fluorescence area, respectively. Solutions should be optically dilute to avoid inner filter effects. The Rhodamine 6G was used as the reference sample, which possessed a known quantum yield of 0.94[35].

Detection of singlet oxygen quantum yields

The quantum yields of singlet oxygen (Φ_Δ) of **I, H, OMe, and NO2** were studied using diphenylisobenzofuran (DBPF) as a chemical quencher[36]. Briefly, a mixture of the BODIPY dye (absorption ~0.06 at 515 nm in EtOH) and the DPBF (absorption ~1.0 at 424 nm in EtOH) was irradiated with green laser light (λ_{max} = 520 nm). The photooxidation of DPBF was monitored between 0~70 min depending on the efficiency of the BODIPY. The singlet oxygen quantum yield was calculated using hematoporphyrin (HP) as the reference with a yield of 0.53 in ethanol according to the following equation:

$$\Phi_\Delta^S = \frac{k_S}{k_R} \times \Phi_\Delta^R$$

Where *k* is the slope of the photodegradation rate of DPBF, S means the sample, R represents the reference, and is the reference's singlet oxygen quantum yield.

Quantum chemical calculations

Molecular structure optimizations for BODIPY derivatives were carried out using density functional theory (DFT), and their electronic states were calculated using time-dependent DFT (TD-DFT). For H, OMe, and NO2, the b3lyp functional of the Gaussian 16 program package and 6-31G(d) basis sets were chosen. For I, due to the heavy iodine atom, lanl2dz basis sets were chosen instead. All calculations were carried out in water solvent environment. The lactose-tethered triazole moiety attached to the a-position of the BODIPY core was confirmed to have a negligible influence on calculation results (Figure S2) and therefore was replaced by a hydrogen atom for simplicity.

Preparation of BODIPY nanoparticles (NPs)

The stock solution of each BODIPY dyes in THF (0.5 $mg.ml^{-1}$) was prepared, then 50 μL of stock solution was slowly added to 5 mL of water. The mixture was stirred overnight to evaporate all of THF naturally to yield the designed nanoparticles for further experiment.

Cells and cell culture

HeLa (human cervix adenocarcinoma), Huh7 (human liver carcinoma) cells were obtained from the Korean Cell Line Bank. The cells were maintained in RPMI 1640 medium (Gibco, Carlsbad, CA, USA) supplemented with 10% heat-inactivated fetal bovine serum (FBS) and antibiotics (100 U/mL penicillin and 100 mg/mL streptomycin) at 37 ºC in a humidified 5% CO_2 incubator.

Cell proliferation assay

Cell proliferation was studied using CellTiter 96 ® Aqueous One Solution Cell Proliferation Assay (Promega, Madison, WI, USA) according to the manufacturer's instructions. Briefly, HeLa and Huh7 (3×10^3 cells/well) were seeded in 96-well plates. After the cells were maintained for 24 h, cells were treated with BODIPY **I, H, OMe, and NO2** at different concentrations (0, 0.25, 0.5, and 1 μM) for 24 h. Following 24 h of incubation, 20 μL MTS [3-(4, 5-dimethylthiazol-2-yl)-5-(3-carboxymethoxyphenyl)-2-(4-sulfophenyl)-2H-tetrazolium] reagent were added to each well and incubated for 4 h at 37°C. The absorbance was determined at 490 nm using an ELISA plate reader (Thermo Fisher Scientific, Inc., Waltham, MA, USA).

Assessment of cellular uptake and cellular imaging

To confirm the cellular uptake and cellular imaging by using the BODIPY **I, H, OMe, and NO2,** Huh-7 cells were incubated with 2 μM of BODIPY **I, H, OMe, and NO2** for 2 h and washed three times with DPBS. After then, the cells were subsequently counterstained with Hoechst 33342 for 10 min. After washing three times with DPBS, the morphologies of Huh-7 cells were taken by an automated live-cell imager (Lionheart

FX, BioTek Instruments, Inc., VT, USA) with 40 x objective lens and fluorescence optics (excitation at 520 nm for BODIPY **I, H, OMe, and NO2** and at 377 nm for Hoechst 33342, and emission at 535 nm for BODIPY **I, H, OMe, and NO2** and at 447 nm for Hoechst 33342). Cellular images were analyzed using Gen5^{TM} imager software (Ver.3.04, BioTek Instruments, Inc., VT, USA).

Photodynamic anticancer activity assessment.

The HeLa and Huh7cells were seeded at 3 × 10^3 cells/well in a 96-well plate and incubated at 37 °C in 5 % CO_2. After 24 h, the cells were incubated again with various concentrations of BODIPY **I, H, OMe,** and **NO2** (0, 0.25, 0.5, and 1 μM) at 37 °C in 5 % CO_2 for 2 h under dark conditions. After 2 h incubation for uptaking the BODIPY **I, H, OMe,** and **NO2** into the cells, the media in all plates were changed with RPMI 1640 media without phenol red. Irradiation of cells was performed with a green light-emitting diode (LED) using about 9 mW (530 nm, for 20 min, 80%). After irradiation, the cells were incubated for an additional 24 h, and the cell proliferation was measured using CellTiter 96 ® Aqueous One Solution Cell Proliferation Assay as the same method for the cytotoxicity described above.

Cellular uptake using flow cytometry

The cells (HeLa and Huh7) were seeded at 1×10^5 cells/well in 6-well plate. After 24 h incubation at 37°C in 5 % CO_2, the BODIPY **I, H, OMe,** and **NO2** (2 μM) were treated with cells for 2 h. Then, the cell were washed with phosphate buffered saline and analyzed using flow cytometry FC500 (Beckman coulter, CA, USA).

Statistical Analysis

All results are expressed as the means ± standard deviations and were compared by one-way analysis of variance (ANOVA followed by Tukey's analysis with Prism GraphPad 6 software (San Diego, CA, USA). A significance level was set at $p<0.05$.

Results And Discussion

Synthesis and photophysical characterization of BODIPY NPs

The process used to synthesize the four BODIPY PSs (I, H, OMe, and NO_2) functionalized with lactose-tethering triazole is outlined in Figure 1. The detailed procedure is provided in the Supporting Information section.

Compounds 1a–d were synthesized via condensation reactions using 3-ethyl-2, 4-dimethyl pyrrole with 4-iodobenzoyl chloride and benzaldehyde derivatives, which yielded compounds 1a and 1b–d, respectively. Compounds 2a–d modified with alkyl azide at the 3-methyl position of the BODIPY core were obtained in the same manner[29]. Cu(I)-catalyzed alkyne–azide cycloaddition reactions (CuAAC) were performed with compounds 2a-d and propargyl lactoside to obtain the final compounds

BODIPY I, H, OMe, and NO_2, respectively. The final BODIPY PSs were fully characterized by ^1H, ^{13}C NMR, and HR-MS, as shown in Fig. S12-25.

A series of water-dispersible NPs, namely I-NPs, H-NPs, OMe-NPs, and NO_2-NPs, were obtained from the corresponding BODIPY PSs I, H, OMe, and NO_2 in aqueous solution, respectively, after complete evaporation of tetrahydrofuran (THF).

The hydrodynamic diameters of the obtained BODIPY NPs in aqueous solution were determined using dynamic light scattering (DLS) measurements. As shown in Figure 2a,b and Figure S1, the average diameters of the H, I, OMe, and NO_2-NPs were approximately 71.3, 79.8, 90.5, and 100.7 nm, respectively. The morphology and size of BODIPY NPs were also examined by transmission electron microscopy (TEM), which revealed their spherical morphology and average diameter of approximately 20–30 nm (Fig. 2a and 2b). Notably, the size of the fully hydrated BODIPY NPs as measured by DLS might be larger than that determined in the dried state from TEM. Many water molecules appeared to be entrapped within the BODIPY NPs via interactions with hydrophilic lactose segments.

The optical characteristics of the BODIPY dyes were investigated using UV/Vis absorption and fluorescence spectrometry (Fig. 2c,d and Tab. 1). All of the synthesized BODIPY derivatives showed typical spectra, with a robust $S_0 \rightarrow S_1$ ($\pi \rightarrow \pi^*$) transition band around 518-524 nm, an absorption coefficient of 42400–49500 $M^{-1} \cdot cm^{-1}$ from the boradiazaindacene chromophore,[30,31] and a weak broad band around 350-400 nm corresponding to the $S_0 \rightarrow S_2$ ($\pi \rightarrow \pi^*$) transition, which can be attributed to the out-of-plane vibrations of the aromatic skeleton[3,32]. The iodine (-I) and methoxy ($-OCH_3$) substituents incorporated into the *meso*-phenyl of BODIPY resulted in almost the same absorption and emission spectra as BODIPY H, indicating that these substituents have a negligible effect on the photophysical properties of the BODIPY cores[29]. The BODIPY dyes with H, I, and OMe exhibited a high Φ_F of approximately 45%–50% (Table 1), which is usually recorded for BODIPY derivatives[29]. Of note, the values of Φ_F remained high despite the BODIPY dyes being modified with the lactose-tethering triazole substituent[17,33]. However, the nitro substituent ($-NO_2$) appeared to have a more significant influence on the photophysical properties of the BODIPY dye. The absorption spectrum of compound NO_2 exhibited a red-shift of approximately 6 nm relative to that of H.

Table 1. The photophysical and photosensitizing properties of BODIPY **I**, **H**, **OMe**, and **NO_2** in MeOH

	I	H	OMe	NO_2
λ_{ab} (nm)[a]	522	518	520	524
λ_{em} (nm)[a]	535	533	530	534
ε (10^3 $M^{-1}cm^{-1}$)[a]	45.2	42.4	44.3	49.5
Φ_F (%)[b]	45.3	50.6	49.2	1.35
Φ_Δ[c]	10	3.7	7.3	0.9

(a) Absorption and fluorescence data measured using methanol. (b) Fluorescence quantum yields were determined using rhodamine 6G in methanol as the standard (Φ_f = 0.94[35]). (c) Singlet oxygen quantum yields were determined by the DPBF bleaching method, using HP in ethanol as a reference (Φ_Δ = 0.53)[36].

As shown in Table S1, the emission intensities and Φ_F of NO_2 were strongly quenched in protic polar solvents, exhibiting Φ_F of 3.46% in ethanol and 1.35% in methanol compared with 38% in THF. The intense emission observed in THF corresponds to the fluorescence from the local excited (LE) state of the BODIPY subunit. In contrast, fluorescence is strongly quenched in a polar methanol solution, owing to a low-emissivity CT state[34]. This phenomenon is expected because the PeT mechanism competes with fluorescence[22,25,26]. Details of the photophysical studies are presented in the theoretical calculation section.

Singlet oxygen generation

The singlet oxygen ($^1O_2$) generation capabilities of **I**, **H**, **OMe,** and **NO_2** were assessed in air-saturated ethanol under irradiation at 520 nm. A commercial $^1O_2$ probe, 1,3-diphenylisobenzofuran (DPBF), was used as an indicator, and hematoporphyrin (HP-$\Phi\Delta$= 0.53 in EtOH) was used as the reference[37].

As shown in Figs. 3a,b,c and S3, the absorbance of DPBF at 414 nm decreased gradually in the presence of the BODIPY dyes under continuous light irradiation. According to the linear relationship of the decay curves (Fig. 3d), the $^1O_2$ quantum yields ($\Phi\triangle$) of **I**, **H**, **OMe,** and **NO_2** were 10%, 3.7%, 7.3%, and 0.9%, respectively (Table 1). Thus, the most robust $^1O_2$ generation ability of **I** among the series of PS suggested that the additional heavy iodine atom on the *meso*-phenyl of BODIPY induced spin-orbit perturbations on the molecules and significantly influenced its superior capability to generate singlet oxygen, as shown by the faster reducing rate of DPBF absorbance bands and a higher $\Phi\triangle$ than that of the other dyes. However, the incorporation of the electron-donating group (-OCH_3) at the *meso*-phenyl of BODIPY played an essential role in enhancing the $^1O_2$ generation of **OMe**. In contrast, the introduction of a strong electron-withdrawing group (-NO_2) did not lead to an efficient $\Phi\triangle$ of BODIPY **NO_2** in a polar solvent (ethanolic solution). However, as shown in Figure S4a, $\Phi\triangle$ could be

enhanced to 3% in a less polar solvent (THF). Such finding indicates that the triplet state of BODIPY **NO_2** is strongly affected by the polarity of the media (the details are presented in the theoretical calculation). These results collectively indicate that both iodinated- *meso*-phenyl BODIPY **I** and heavy-free atom BODIPY **OMe** achieved an elevated $^1O_2$ under LED illumination that facilitated singlet oxygen generation, demonstrating their potential use as efficient photosensitizers for PDT.

Theoretical characterization of the BODIPY derivatives

To determine the effect of *meso*-phenyl substituents on the electronic structure of BODIPY derivatives, density functional theory (DFT) calculations were performed (see Methods for computational details). For BODIPY **OMe**, as depicted in Fig. 4, HOMO-1 is mainly located on methoxyphenyl (MPh). In contrast, the LUMO is fully localized on the BODIPY (BDP), implying that upon the generation of the singlet excited state by photoexcitation, PeT may occur, leading to the CT state, $^1[BDP^{\bullet-}–MPh^{\bullet+}]$. This process enhances the triplet state formation efficiency, as demonstrated by the significant increase in of **OMe**, compared with **H**. The CT state was approximately 0.2 eV higher in energy than the singlet excited state (Table S2). However, Filatov et al. showed that even if the energy of the CT state is greater than that of the singlet excited state, PeT and the subsequent triplet state formation can occur, with a propensity that the efficiency of the processes reduces with increasing energy gap[22]. Hence, despite the reversal of the state energy, PeT is viewed as a valid mechanism for **OMe**, which facilitates the generation of the triplet state and $^1O_2$.

The electron-withdrawing nitro group existing in **NO_2** causes nitrophenyl (NPh) to act as an electron acceptor, while BODIPY becomes an electron donor, as demonstrated by the HOMO and LUMO localized on BODIPY and nitrophenyl, respectively (Fig. 5). Therefore, in **NO_2**, PeT may produce $^1[BDP^{\bullet+}–NPh^{\bullet-}]$. Unlike **OMe**, this CT state lies between the singlet and triplet excited states (Table S2). The results of the DFT calculations, in conjunction with the solvent dependency of , clearly confirm the existence of PeT in **NO_2**; however, this does not lead to efficient triplet state formation, as reflected by the very low of this compound.

For donor-acceptor-type BODIPY dyads, comparing the frontier orbital energies of donor and acceptor units is beneficial for explaining electron movement during the PeT process[34]. This approach applies to **NO_2** because, in its optimized geometry, the two subunits are oriented almost perpendicular and can be considered as two independent functional groups. In this context, to elucidate the unexpected decoupling between PeT and the triplet state formation observed for **NO_2**, the HOMO/LUMO energies of hexaalkyl-substituted BODIPY and nitrobenzene were calculated and compared (see Fig. 5a).

As illustrated in Fig. 5b, ISC from $^1[BDP^{\bullet+}–NPh^{\bullet-}]$ to $^3[BDP^{*}–MPh]$ requires the back transfer of an electron from $LUMO_{NPh}$ to $LUMO_{BDP}$, following the conversion of its spin; this process is known as the radical pair ISC (RP-ISC). However, DFT calculations revealed that $E(LUMO_{BDP}) > E(LUMO_{NPh})$ (Fig. 5a), demonstrating that for **NO_2**, back electron transfer (BeT) is an energetically unfavorable process. These

findings agree with those of Zhao et al., who explored redox potentials for energetic comparison of frontier orbitals[38]. In addition, electron spin conversion, which must precede the above process, is often forbidden for directly linked donor-acceptor systems, such as **NO_2**. Hence, ^{1}[BDP$^{\bullet+}$–NPh$^{\bullet-}$] of **NO_2** is most likely to decay nonradiatively to the ground state. However, whether this dissipation occurs directly or via the formation of ^{3}[BDP–NPh*] remains unclear.

These results are consistent with those of Qi et al[8]. The electronic properties of the *meso*-substituent on the BODIPY core, particularly the introduction of a suitable electron-donating group, could be fine-tuned to control the efficiency of singlet oxygen formation. These results suggest that BODIPY **OMe** can be used as a theranostic agent for cancer treatment.

Cellular uptake and cell-imaging of BODIPY NPs

Cellular uptake behaviors of the BODIPY NPs against Huh-7 (human liver carcinoma) and HeLa (human cervix adenocarcinoma) cells were measured and compared by flow cytometry analysis. First, the cells were incubated with 2.0 μM of the BODIPY PSs for 2 h at 37 °C; then, the treated cells were collected and subjected to fluorescence-activated cell sorting (FACS). As depicted in Fig. 6b,c, these BODIPY NPs exhibited higher selectivity for Huh-7 cells than HeLa cells. The mean fluorescence of liver cancer cells treated with **I**, **H**, **OMe**, and **NO_2-NPs** was approximately 4.6-, 6.2-, 6.1-, and 4-fold higher than that of the treated HeLa cells (Fig. 6b,c and Tab. S3). Such finding is due to the high density of ASGP receptors on the surface of liver cancer cells, which can bind BODIPY NPs containing galactose residues and be successfully internalized into Huh-7 cells via receptor recognition[39,40], which is consistent with our previous report[17].

Lactose modification can provide BODIPY NPs with potential applications in specific liver cancer imaging ability. To evaluate the potential application of the fluorescent dye for cell imaging, liver cancer Huh-7 cells were treated with these dyes for 2 h and imaged by confocal microscopy. Hoechst 33342, a fluorescent stain commonly used to visualize the nucleus, was used to confirm fluorescent dye localization within the cells. As shown in the cellular images (Fig. 6a), the targeting BODIPY NPs could be effectively transported into Huh-7 cells, which was mediated by galactose receptors, after cultivation for 2 h and firmly gathered in the cytoplasm and perinuclear region. Hoechst 33342 resulted in blue fluorescence in the nucleus of Huh-7 cells, and the merged image revealed that these BODIPY NPs could specifically bind to Huh-7 cells and localize in their cytoplasm. Therefore, these BODIPY NPs can effectively distinguish the cytoplasm of Huh-7 cells from the nucleus.

Huh-7 cells cultured with **H**, **I**, and **OMe-NPs** showed stronger fluorescence, whereas those cultured with **NO_2-NPs** displayed weaker fluorescence; this is caused by the cellular uptake of **NO_2-NPs** being the lowest, consistent with the FACS results. Additionally, as mentioned above, **NO_2-NPs** exhibited PeT in polar media, resulting in the CT state, which inhibits fluorescence. As a result, **NO_2-NPs** appeared darker in the cell-imaging than the other compounds.

Light-induced cytotoxicity of BODIPY NPs against cancer cells

The biocompatibility of **I**, **H**, **NO_2**, and **OMe-NPs** with Huh-7 and HeLa cells was determined using MTS assays. As shown in Figure 7a and Figure S5a, there was no cytotoxicity in any of the tested cells, and more than 97% of both Huh-7 and HeLa cells survived after 24 h of incubation. Thus, all water-soluble BODIPY PSs below a dose of 1 μM had good biocompatibility and did not induce severe cytotoxicity in fibroblasts and cancer cells, implying that BODIPY **I**, **H, NO_2**, and **OMe-NPs** could be used in the light cytotoxicity test.

For the efficient production of ROS, HeLa and Huh-7 cells were exposed to 530 nm laser irradiation at an extremely low energy of 8.6 J·cm^{-2}, and the in vitro phototoxicity of PDT was assessed. First, there was no significant variance when HeLa and Huh-7 cells were cultured with RPMI containing 1 μM of **H** and **NO_2-NPs**, not only under dark conditions but also under irradiation; this is because of their low singlet oxygen quantum yield, as mentioned above. When exposed to LED light, **I** and **OMe-NPs** resulted in high phototoxicity to tumor cells and negligible cell toxicity in the dark, as shown in Figure 7b and Figure S5b. Cell viability evidently decreased as the concentration of these BODIPY NPs increased. Furthermore, when HeLa cells were exposed to light in the presence of 1 μM of **OMe** and **I-NPs**, cell viability decreased by approximately 78% and 83%, respectively, while Huh-7 cells died by up to 89% and 97.7%, respectively, indicating their efficient PDT targeting ability. Besides, the half-lethal dose (IC50) of **OMe-NPs** for HeLa and Huh-7 cell lines was 0.62 and 0.52 μM, respectively. Notably, when exposed to light, the lactose-tethered BODIPY **OMe** and **I-NPs** killed more Huh-7 cells than HeLa cells, with IC50 values of 0.51 and 0.26 μM, respectively. These results demonstrate that BODIPY **I** and **OMe-NPs** provide better treatment efficacy with relatively low irradiation intensity than **H** and **NO_2-NPs**.

Conclusion

Herein, we designed and synthesized a series of lactose-functionalized BODIPY PSs with different substituent groups at the *meso*-position of the BODIPY core as cancer-targeted theragnostic agents for imaging and PDT. These BODIPY PSs could aggregate into nanoparticles (**I-, H-, NO_2-**, and **OMe-NPs**) in an aqueous solution and displayed a uniform size and shape, as determined by TEM and DLS. The fluorescence quantum yields of BODIPY **I**, **H**, and **OMe** were remarkably high, whereas that of BODIPY **NO_2** was significantly lower due to the PeT process in polar media. Among the four BODIPY photosensitizers, BODIPY **I** demonstrated high efficiency of singlet oxygen generation caused by the heavy atom effect due to the presence of an iodine atom, while BODIPY **OMe** containing an electron-donating methoxy group at the *meso*-phenyl moiety enhanced the ISC. In contrast, the withdrawing electron (NO_2) caused a marked reduction in both the fluorescence and singlet oxygen of **NO_2** due to PeT in the polar media. The cell experiments demonstrated that the water-soluble BODIPY NP series showed good biocompatibility and cancer-specific fluorescence imaging ability. Notably, BODIPY **OMe** and **I-NPs** presented excellent phototoxicity against cancer cells, especially, liver cancer Huh-7 cells. The

biocompatible BODIPY NPs have proven to be promising for developing highly efficient theragnostic agents for imaging-guided PDT for cancer treatment.

Declarations

Acknowledgements

This work was performed with financial support from the research funds provided by Chosun University in 2021.

Author contributions

D.K.M, H.J.K designed the protocol. D.K.M, I.W.B, and T.P.V carried out the experiments. J.L conducted cell experiments. C.K studied computational modeling work. S.C, J.Y, and H.J.K supported and advised the experiments. D.K.M, J.Y, and H.J.K wrote the manuscript. All authors discussed the results and commented on the manuscript.

Competing Interests

The authors declare no competing financial interests.

References

1. Allison, R. R. & Sibata, C. H. Oncologic photodynamic therapy photosensitizers: a clinical review. *Photodiagnosis Photodyn Ther*, **7**, 61–75 (2010).
2. Kamkaew, A. *et al.* BODIPY dyes in photodynamic therapy. *Chem Soc Rev*, **42**, 77–88 (2013).
3. Awuah, S. G. & You, Y. Boron dipyrromethene (BODIPY)-based photosensitizers for photodynamic therapy.*RSC Advances***2**(2012).
4. Kue, C. S. *et al.* Recent strategies to improve boron dipyrromethene (BODIPY) for photodynamic cancer therapy: an updated review. *Photochem Photobiol Sci*, **17**, 1691–1708 (2018).
5. Turksoy, A., Yildiz, D. & Akkaya, E. U. Photosensitization and controlled photosensitization with BODIPY dyes. *Coord. Chem. Rev*, **379**, 47–64 (2019).
6. Yuan, P. *et al.* Oxygen self-sufficient fluorinated polypeptide nanoparticles for NIR imaging-guided enhanced photodynamic therapy. *J Mater Chem B*, **6**, 2323–2331 (2018).
7. Liu, L., Fu, L., Jing, T., Ruan, Z. & Yan, L. pH-Triggered polypeptides nanoparticles for efficient BODIPY imaging-guided near infrared photodynamic therapy. *ACS Appl Mater Interfaces*, **8**, 8980–8990 (2016).
8. Qi, S., Kwon, N., Yim, Y., Nguyen, V. N. & Yoon, J. Fine-tuning the electronic structure of heavy-atom-free BODIPY photosensitizers for fluorescence imaging and mitochondria-targeted photodynamic therapy. *Chem Sci*, **11**, 6479–6484 (2020).

9. Bui, H. T. *et al.* Effect of substituents on the photophysical properties and bioimaging application of BODIPY rerivatives with triphenylamine substituents. *J Phys Chem B*, **123**, 5601–5607 (2019).
10. Guo, Z. *et al.* Bifunctional platinated nanoparticles for photoinduced tumor ablation. *Adv Mater*, **28**, 10155–10164 (2016).
11. Takatoshi Yogo, Y. U., Ishitsuka, Y., Maniwa, F. & Nagano, T. Highly efficient and photostable photosensitizer based on BODIPY chromophore. *J. Am. Chem. Soc.* 2005, 127, 12162–12163 **127**, 12162–12163 (2005).
12. Mark Wainwright, D. A. P., Lesley Rice, S. M. & Burrow Jack Waring. Increased cytotoxicity and phototoxicity in the methylene blue series via chromophore methylation. *Journal of Photochemistry and Photobiology B: Biology*, **40**, 233–239 (1997).
13. Plaetzer, K., Krammer, B., Berlanda, J., Berr, F. & Kiesslich, T. Photophysics and photochemistry of photodynamic therapy: fundamental aspects. *Lasers Med Sci*, **24**, 259–268 (2009).
14. Kim, B. *et al.* In vitro photodynamic studies of a BODIPY-based photosensitizer. *European Journal of Organic Chemistry*, **2017**, 25–28 (2016).
15. Zou, J. *et al.* BODIPY derivatives for photodynamic therapy: influence of configuration versus heavy atom effect. *ACS Appl Mater Interfaces*, **9**, 32475–32481 (2017).
16. Wang, Z. *et al.* BODIPY-doped silica nanoparticles with reduced dye leakage and enhanced singlet oxygen generation. *Sci Rep*, **5**, 12602 (2015).
17. Khuong Mai, D. *et al.* Synthesis and photophysical properties of tumor-targeted water-soluble BODIPY photosensitizers for photodynamic therapy.*Molecules***25**(2020).
18. Aoife Gorman, J. K., Caroline, O. S., Kenna, T., Gallagher, W. M. & Donal, F. O'Shea. In vitro demonstration of the heavy-atom effect for photodynamic therapy. J. Am. Chem. Soc. 2004, 126, 10619–10631 **126**, 10619–10631.
19. Lu, S. *et al.* PEGylated dimeric BODIPY photosensitizers as nanocarriers for combined chemotherapy and cathepsin B-activated photodynamic therapy in 3D tumor spheroids. *ACS Applied Bio Materials*, **3**, 3835–3845 (2020).
20. Chen, H., Bi, Q., Yao, Y. & Tan, N. Dimeric BODIPY-loaded liposomes for dual hypoxia marker imaging and activatable photodynamic therapy against tumors. *J Mater Chem B*, **6**, 4351–4359 (2018).
21. Ucuncu, M. *et al.* BODIPY-Au(I): a photosensitizer for singlet oxygen generation and photodynamic therapy. *Org Lett*, **19**, 2522–2525 (2017).
22. Filatov, M. A. *et al.* Control of triplet state generation in heavy atom-free BODIPY-anthracene dyads by media polarity and structural factors. *Phys Chem Chem Phys*, **20**, 8016–8031 (2018).
23. Callaghan, S., Filatov, M. A., Savoie, H., Boyle, R. W. & Senge, M. O. In vitro cytotoxicity of a library of BODIPY-anthracene and -pyrene dyads for application in photodynamic therapy. *Photochem Photobiol Sci*, **18**, 495–504 (2019).
24. Filatov, M. A. Heavy-atom-free BODIPY photosensitizers with intersystem crossing mediated by intramolecular photoinduced electron transfer. *Org Biomol Chem*, **18**, 10–27 (2019).

25. Li, L., Nguyen, J. H. B. & Burgess, K. Syntheses and spectral properties of functionalized, water-soluble BODIPY derivatives. *J. Org. Chem. 2008, 73, 1963–* 1970 **73**, 1963–1970 (2008).
26. Dorh, N. *et al.* BODIPY-based fluorescent probes for sensing protein surface-hydrophobicity. *Sci Rep*, **5**, 18337 (2015).
27. Hisato Sunahara, Y. U., Kojima, H. & Nagano, T. Design and synthesis of a library of BODIPY-based environmental polarity sensors utilizing photoinduced electron-transfer-controlled fluorescence ON/OFF switching. *J. Am. Chem. Soc.* 2007, 129, 5597–5604 **129**, 5597–5604 (2007).
28. Kim, T. H., Park, I. K., Nah, J. W., Choi, Y. J. & Cho, C. S. Galactosylated chitosan/DNA nanoparticles prepared using water-soluble chitosan as a gene carrier., **25**, 3783–3792 (2004).
29. Ulrich, G., Ziessel, R. & Haefele, A. A general synthetic route to 3,5-substituted boron dipyrromethenes: applications and properties. *J Org Chem*, **77**, 4298–4311 (2012).
30. Shilei Zhu, J. Z., Vegesna, G., Luo, F. T., Green, S. A. & Liu, H. Highly water-soluble neutral BODIPY dyes with controllable fluorescence quantum yields. *Org. Lett*, **13**, 438–441 (2011).
31. Vu, T. T. *et al.* Understanding the spectroscopic properties and aggregation process of a new emitting boron dipyrromethene (BODIPY). *The Journal of Physical Chemistry C*, **117**, 5373–5385 (2013).
32. Sun, H. *et al.* Excellent BODIPY dye containing dimesitylboryl groups as PeT-based fluorescent probes for fluoride. *The Journal of Physical Chemistry C*, **115**, 19947–19954 (2011).
33. Papalia, T. *et al.* Cell internalization of BODIPY-based fluorescent dyes bearing carbohydrate residues. *Dyes and Pigments*, **110**, 67–71 (2014).
34. Filatov, M. A. *et al.* Generation of triplet excited states via photoinduced electron transfer in meso-anthra-BODIPY: fluorogenic response toward singlet oxygen in solution and in vitro. *J Am Chem Soc*, **139**, 6282–6285 (2017).
35. Douglas & Magde R.W.a.P.G.S. Fluorescence quantum yields and their relation to lifetimes of rhodamine 6G and fluorescein in nine solvents: improved absolute standards for quantum yields. Photochemistry and Photobiology, 2002, 75(4): 327–334 **75**, 327–334 (2002).
36. Wolfgang Spiller, H. K., Dieter Wo¨hrle, S. & Hackbarth Beater Ro¨der and Gu¨nter Schnurpfeil. Singlet oxygen quantum yields of different photosensitizers in polar solvents and micellar solutions. Journal of Porphyrins and Phthalocyanines, Vol. 2, 145–158 (1998*)* **2**, 145–158 (1998).
37. Liane, M. *et al.* Baptista. Protoporphyrin IX nanoparticle carrier: preparation, optical properties, and singlet oxygen generation. Langmuir 2008, 24, 12534–12538 **24**, 12534–12538 (2008).
38. Hu, W. *et al.* Can BODIPY-electron acceptor conjugates act as heavy atom-free excited triplet state and singlet oxygen photosensitizers via photoinduced charge separation-charge recombination mechanism? *The Journal of Physical Chemistry C*, **123**, 15944–15955 (2019).
39. Lu, Z. *et al.* Water-soluble BODIPY-conjugated glycopolymers as fluorescent probes for live cell imaging.*Polymer Chemistry***4**(2013).
40. Liu, L., Ruan, Z., Li, T., Yuan, P. & Yan, L. Near infrared imaging-guided photodynamic therapy under an extremely low energy of light by galactose targeted amphiphilic polypeptide micelle

encapsulating BODIPY-Br2. *Biomater Sci*, **4**, 1638–1645 (2016).

41. Khuong Mai, D. *et al.* Aggregation-induced emission of tetraphenylethene-conjugated phenanthrene derivatives and their bio-imaging applications.*Nanomaterials (Basel)***8**(2018).

Figures

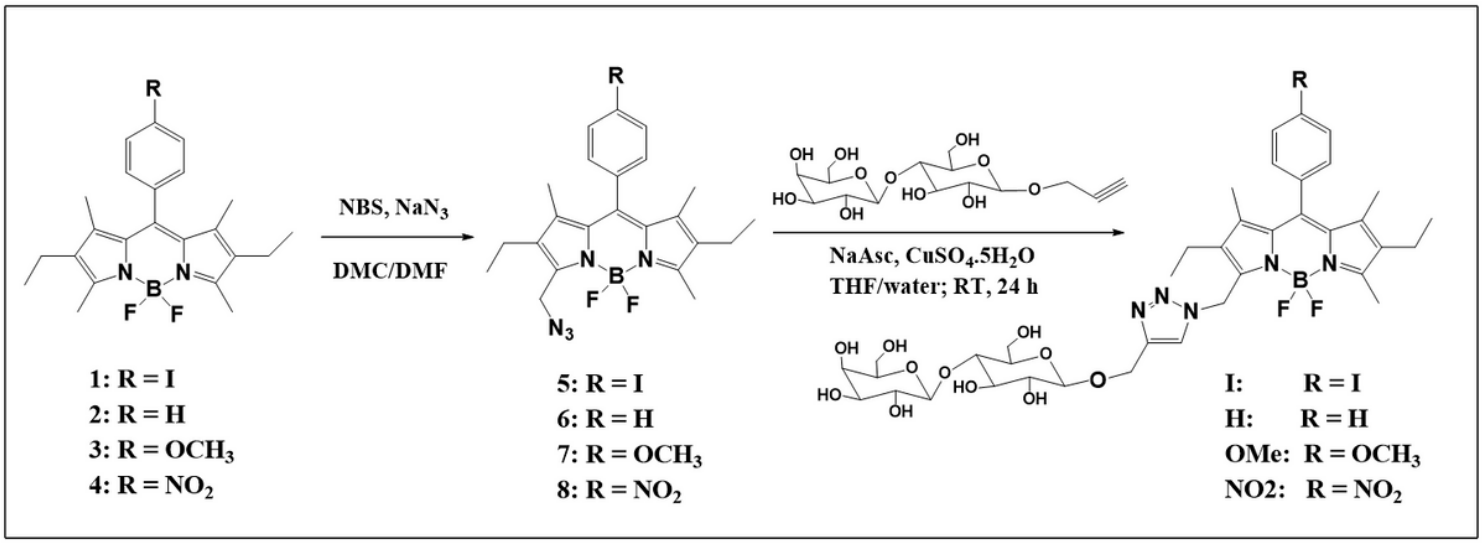

Figure 1

The preparation of lactose-functionalized BODIPY PSs with different meso-phenyl substituents

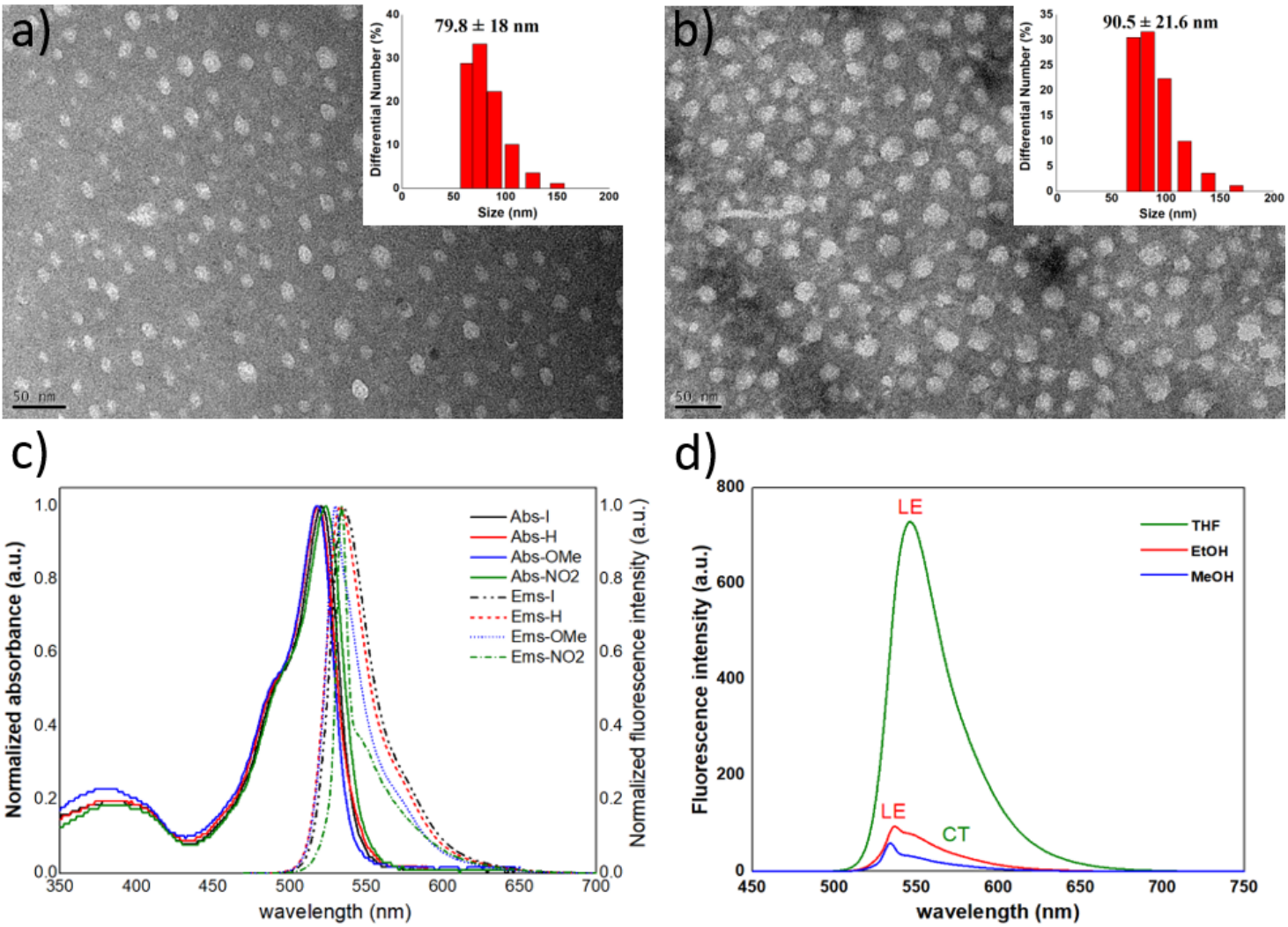

Figure 2

Characterization of BODIPY PSs. TEM images of I-NPs (a) and OMe-NPs (b) (the scale bar: 50 nm). The inset images indicate the sizes of I-NPs and OMe-NPs based on DLS. The normalized absorption and emission spectra of I, H, OMe, and NO2 in methanolic solution at c= 5 μM (c). The emission spectra of BODIPY NO2 in various solvents at c= 5 μM (d). The solutions were excited at their absorption maxima.

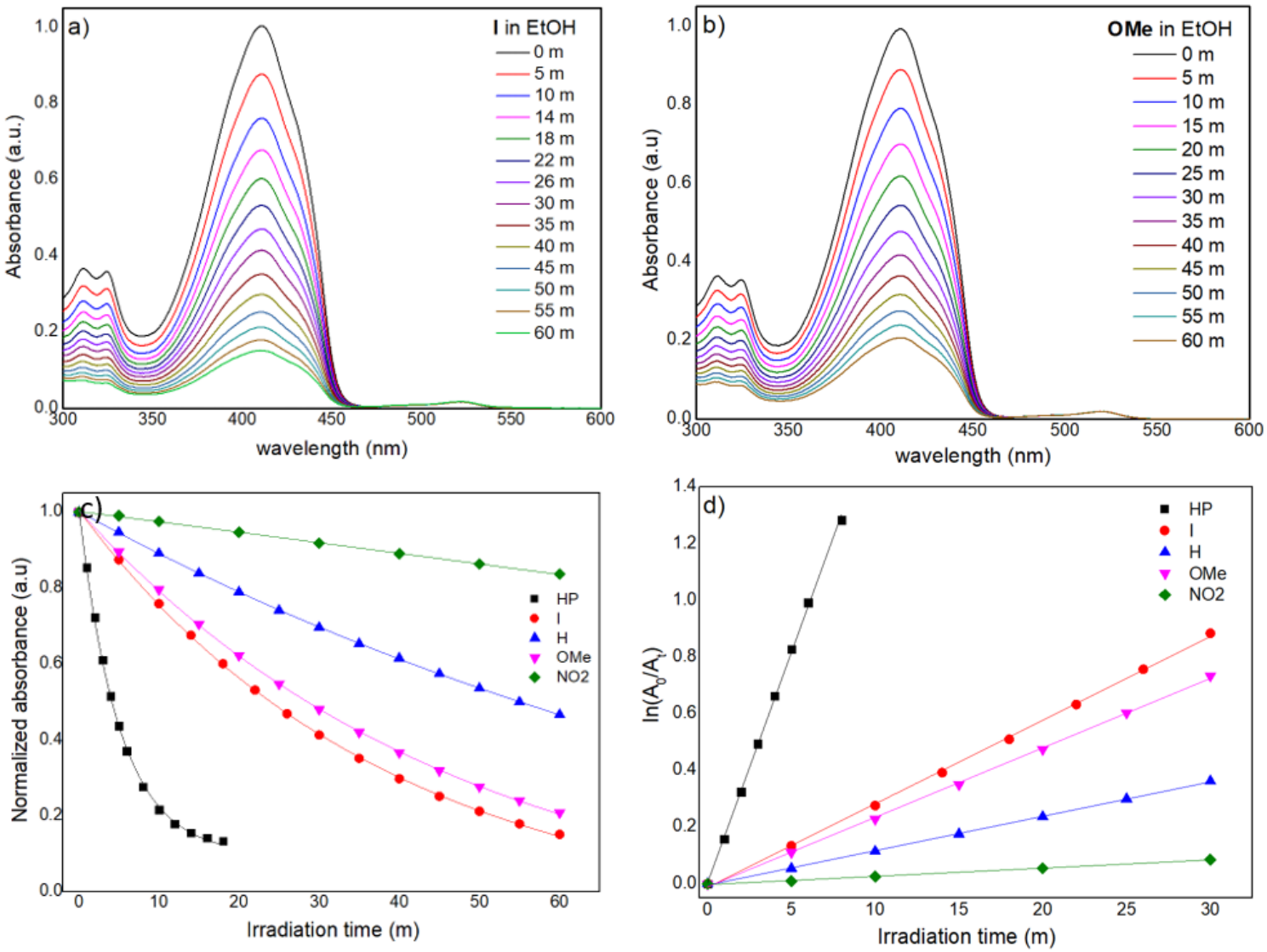

Figure 3

The singlet oxygen (1O2) generation capabilities of BODIPY PSs. Absorption spectra of DPBF upon irradiation in the presence of (a) I and (b) OMe under 520 nm for different times. (c) Plots of the change in absorbance of DPBF at 414 nm at different irradiation times using hematoporphyrin (HP) as the standard in EtOH at room temperature (ΦΔ = 0.53). (d) 1O2 assay using the absorbance attenuation of DPBF in the presence of BODIPY I, H, OMe, and NO2 against HP as the standard in EtOH.

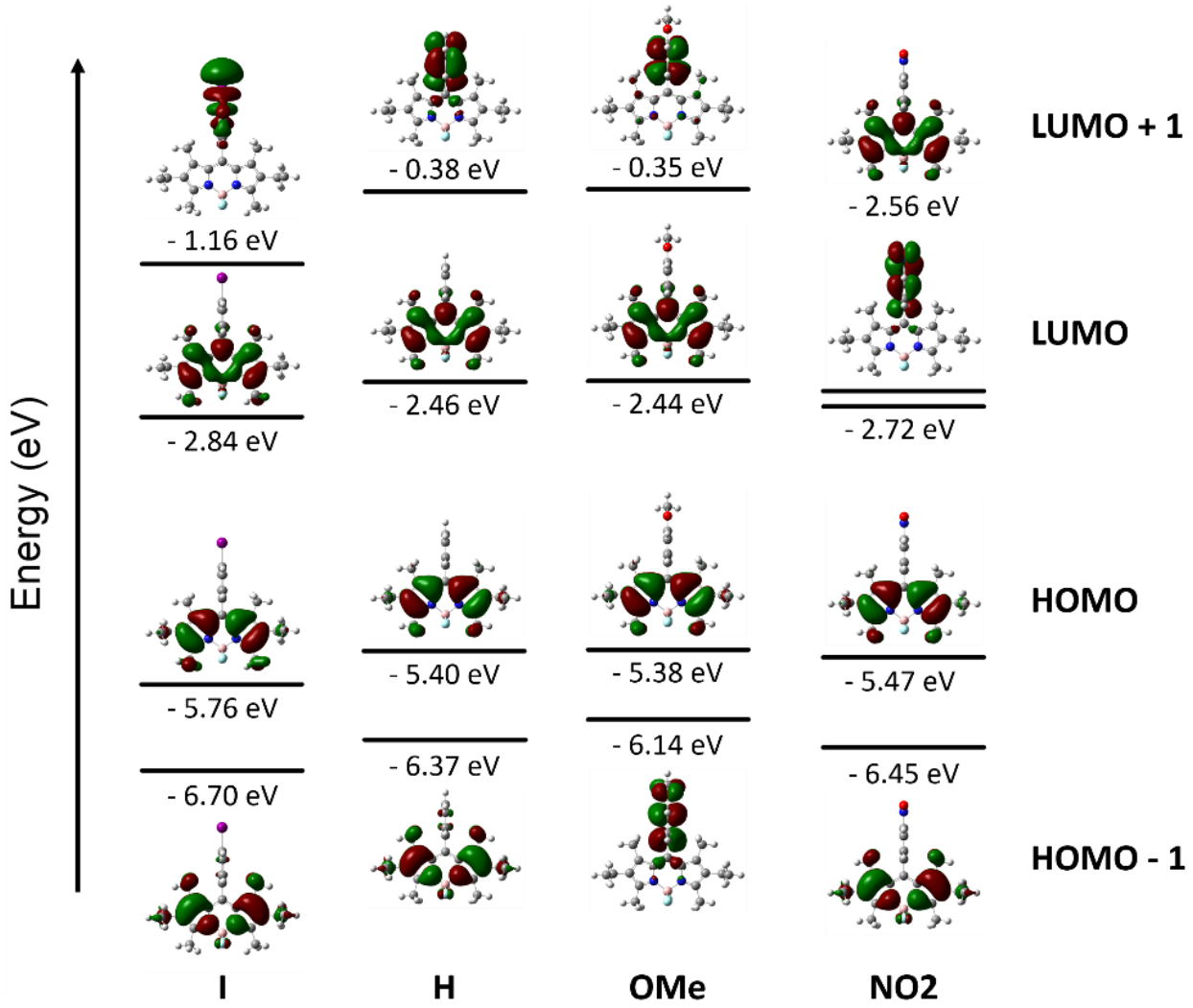

Figure 4

Frontier molecular orbitals and their energies for BODIPY PSs.

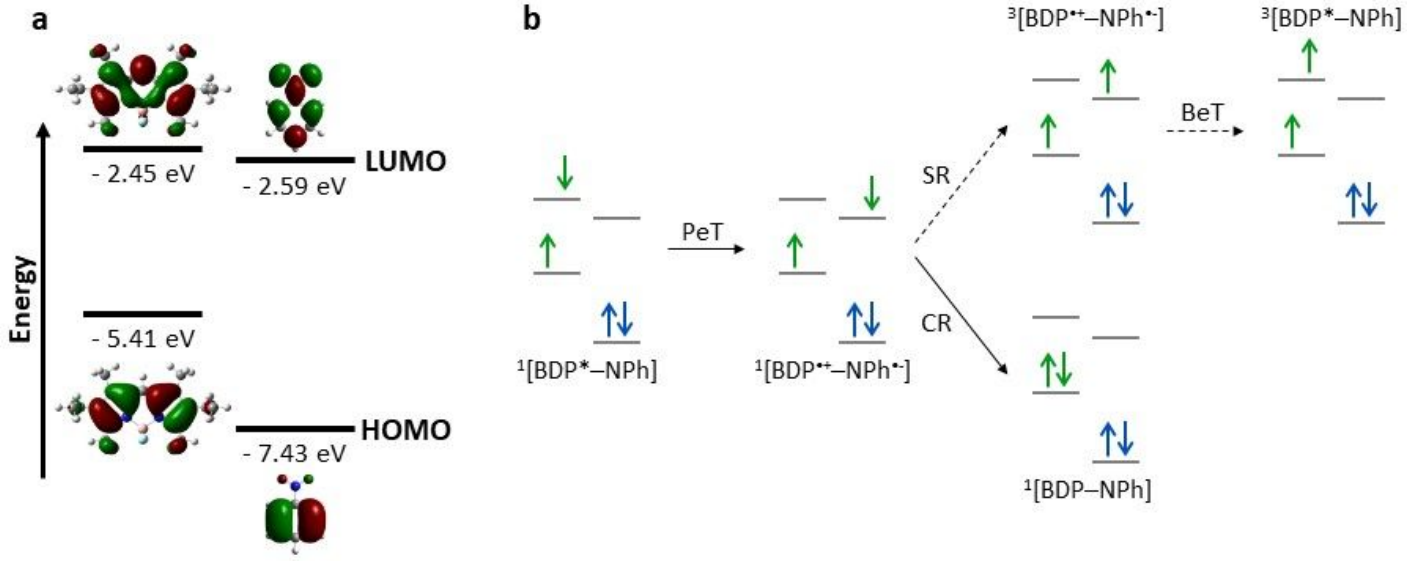

Figure 5

(a) Frontier orbital energies of two subunits of NO2. (b) Schematic of the electron movement required for PeT-mediated triplet state generation in NO2. In (b), SR, CR, and BeT represent spin reversion, charge recombination, and back electron transfer, respectively.

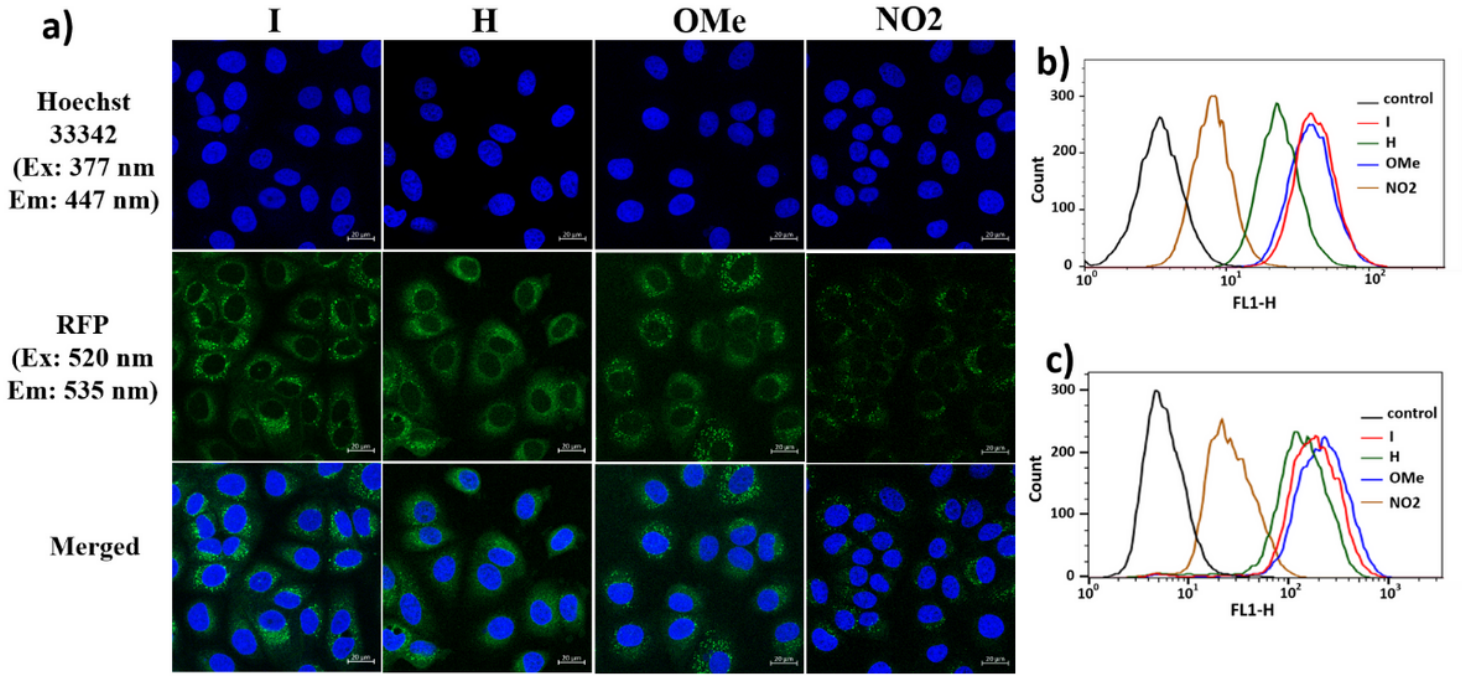

Figure 6

Cell selectivity and imaging of lactose-functionalized BODIPY PSs. Fluorescence images of Huh-7 cells were captured after a 2 h incubation with 2 μM of I, H, OMe, and NO2-NPs. After incubation, cell nuclei were stained with Hoechst 33342 dye for 10 min. Images were captured with a 40× objective lens and fluorescence optics (excitation at 520 nm for I, H, OMe, and NO2-NPs and 377 nm for Hoechst 33342; and emission at 535 nm for I, H, OMe, and NO2-NPs and 447 nm for Hoechst 33342). Scale bar = 20 μm (a). The fluorescence-activated cell sorting (FACS) analysis of HeLa (b) and Huh7 cells (c) treated with 2 μM of BODIPY I, H, OMe, and NO2.The incubation time was 2 h for all BODIPY NPs.

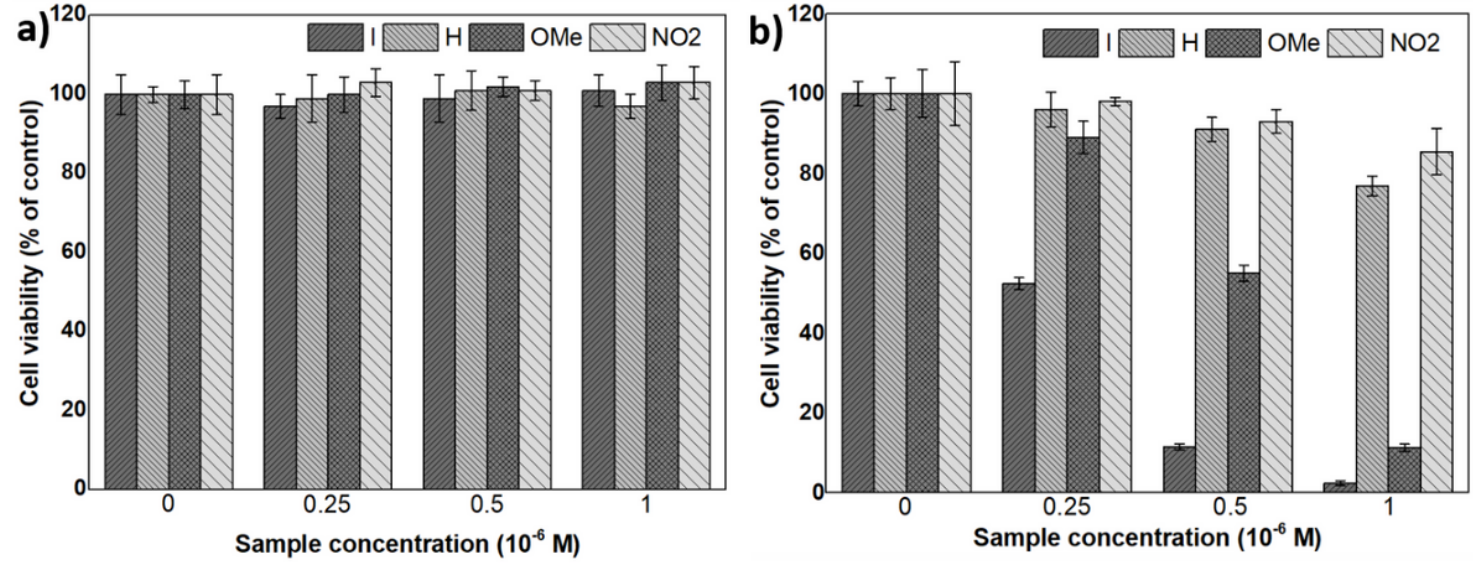

Figure 7

Photodynamic anticancer activities of BODIPY PSs in Huh-7 cells. Cytotoxicity (a) and phototoxicity (b) of BODIPY I, H, NO2, and OMe-NPs in Huh-7 cells (hepatocellular carcinoma) under light irradiation (λirr 530 nm, 8.6 J·cm-2). The cell viabilities were detected using a CCK-8 kit after incubation with I, H, OMe, and NO2-NPs for 24 h under dark conditions. Quantitative data are expressed as mean ± standard deviation (n=4). Statistical significance based on the Student's t-tests was considered as $p<0.005$.

Supplementary Files

This is a list of supplementary files associated with this preprint. Click to download.

- HJKScientificReportSI.pdf